Life-Cycle of Structures and Infrastructure Systems – Biondini & Frangopol (Eds)

Influence of different debonding gap types on mechanical performance of axially compressed CFST stub columns with same debonding arc-length ratio

J.Q. Xue, J.P. Huang, L.Q. He, B. Briseghella & A. Contento
College of Civil Engineering, Fuzhou University, Fuzhou, China
Joint International Research Laboratory of Deterioration and Control of Coastal and Marine Infrastructures and Materials, Fuzhou University, Fuzhou, China

ABSTRACT: The mechanical properties of concrete-filled steel tubular (CFST) members are influenced by the possible debonding gap between the steel tube and concrete core. To investigate this phenomenon, finite element models (FEMs) of the CFST columns with different debonding types, such as the circumferential debonding gap (CDG) and spherical-cap debonding gap (SDG), were established by using ABAQUS. The accuracy of the FEMs was verified comparing the obtained results with experimental ones. The verified FEMs were used to analyze the influence of different debonding types on the mechanical performance of the axially compressed CFST stub columns with the same debonding arc-length ratio (R_D). The results showed that with an increase in R_D, the ultimate load-bearing capacity (N_u) of CFST columns decreased. However, a critical R_D ($R_{D\text{-}cr}$) was found, in fact when the R_D was less than or equals to the $R_{D\text{-}cr}$, the influence of different debonding types on the N_u and failure modes of CFST columns were basically the same. When the R_D was larger than the $R_{D\text{-}cr}$, with an increase in R_D, the N_u of SDG CFST columns decreased linearly, however, the N_u of CDG CFST columns decreased nonlinearly with gradually reduced decrease rates. Finally, it was found that the overall bending, inward and outward buckling in SDG CFST columns were more serious than those in CDG CFST columns.

1 INTRODUCTION

According to the inspections made in arch bridges, debonding gaps can be found between the steel tube and concrete core, which can weaken the combined effect of two materials in CFST (concrete-filled steel tube) structures (Han et al. 2016, Shen et al. 2022, Xue et al. 2010, 2012). Two different types of debonding gaps could be found, which are the circumferential debonding gap (CDG) (Figure 1a) and spherical-cap debonding gap (SDG) (Figure 1b) (Contento et al. 2022, Han et al. 2016, Shen et al. 2022, Xue et al. 2021a).

The main parameters of CDG or SDG are shown in Figures 1a, b, respectively, including the debonding thickness (T_D: T_{CDG} or T_{SDG}), debonding arc-length ratio (R_D: R_{CDG} or R_{SDG}) and debonding length (L_D: L_{CDG} or L_{SDG}). T_{CDG} or T_{SDG} is the maximum distance between the outer surface of the concrete core and the inner surface of the steel tube within the range of CDG or SDG. R_{CDG} or R_{SDG} is the ratio of the arc-length of CDG or SDG to the perimeter of the section ($\theta_{CDG}/2\pi$ or $\theta_{SDG}/2\pi$), where the θ_{CDG} or θ_{SDG} is the angle of CDG or SDG. L_{CDG} or L_{SDG} is the length of CDG or SDG along the direction of the specimen length (L).

Some experimental tests done to investigate the influence of CDG on the mechanical performance of CFST columns have been carried out by choosing the R_{CDG} as the key parameter (R_{CDG} = 0, 0.25, 0.5 and 0.75 (Xue et al. 2012), R_{CDG} = 0 and 0.25 (Xue et al. 2020, 2021b), R_{CDG} = 0 and 0.5 (Shao et al. 2018), R_{CDG} = 0, 0.5 and 1 (Xie. 2018), and R_{CDG} = 0 and 1 (Liao et al. 2011, Han et al. 2016)). It can be found that, with an increase in R_{CDG}, the ultimate load-bearing capacity (N_u) of CFST columns decreased, and the influence of R_{CDG} on the N_u

DOI: 10.1201/9781003323020-335

also decreased. Regarding the failure mode, with an increase in R_{CDG}, the number of local bucking in the range with debonding gap (DG range) increased, the outward local buckling in the range without debonding gap (NDG range) at the mid-height and the elephant-foot shaped buckling near both ends were more obvious (Liao et al. 2011, Han et al. 2016, Xue et al. 2012).

Experimental tests on the influence of SDG on the mechanical performance of CFST columns have been also carried out by choosing the gap ratio of SDG ($\chi_{SDG} = T_{SDG}/D$) as the key parameter. It can be concluded that, with an increase in χ_{SDG}, the N_u of CFST columns linearly decreased. With an increase in χ_{SDG}, the axially compressed CFST columns exhibited clearly local bucking in DG range at failure, and the number of outward local buckling increased at the mid-height; the failure mode of the eccentrically compressed CFST columns changed from inward bending to wavy inward local buckling in DG range. In the literature, there is no research on the influence of R_{SDG} on the mechanical performance of CFST columns.

The influence of CDG or SDG on the mechanical performance of CFST stub columns was analyzed separately in some references (Han et al. 2016, Liao et al. 2011, Shen et al. 2022, Xue et al. 2021). However, the results of CDG or SDG were not compared with each other in the same research. The influence of different debonding gap types on mechanical performance of axially compressed CFST stub columns with the same debonding area was studied by Xue et al. (2022). The results showed that the mechanical performance of CDG or SDG CFST columns with the same debonding area were different.

It is difficult to measure the T_D in real applications. The most accurate detection technology for the T_D is to drill holes on the steel tube, which may damage the steel tube. The knocking method is a nondestructive detection method which can be used to measure the approximate range of debonding gaps to calculate the R_D. Therefore, the R_D should be considered as the key parameter in CFST columns with CDG or SDG. However, there is few research on the influence of different debonding gap types on mechanical performance of axially compressed CFST stub columns with the same R_D based on the knowledge of authors. In this paper, the influence of CDG or SDG on the N_u and failure modes of CFST stub columns with the same R_D were analyzed.

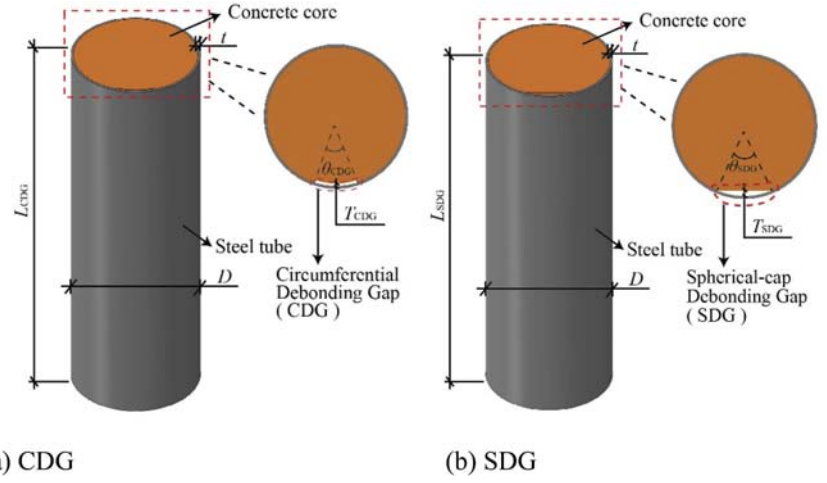

Figure 1. Parameters of debonding gaps.

2 FINITE ELEMENT SIMULATION

2.1 *Finite element modelling*

The steel tube was simulated by shell elements (S4R). The core concrete was simulated by solid elements (C3D8R). The end plates were simulated by discrete rigid elements (R3D4).

The steel tube was simulated by an elastic-plastic model using a stress-strain relation that consists of five stages with Von Mises yield criterion (Han et al. 2007). The damage plasticity model

was used for modelling concrete by using the equivalent stress-strain model proposed by (Han et al. 2007). For concrete in tension, the tensile softening behaviour was set by using the fracture energy model specifying the post failure stress as a tabular function of cracking displacement.

Both the bond and friction actions were considered in the interface modeling between the steel tube and concrete core. For the interface of the cross-sectional area in NDG range, the normal behaviour was simulated with hard contact; the friction coefficient was taken as 0.6 (Xue et al 2022). For the cross-sectional area in DG range (CDG or SDG shown in Figures 1a, b, respectively), both normal contact pressure and tangential shear stress were taken as zero at the beginning. When the inner surface of the steel tube contacted with the outer surface of the concrete core due to the inward buckling in the steel tube, the normal and tangent behaviours of the interface was simulated as the same as the interface of the cross-sectional area in NDG range.

The loading history was applied by using vertical downward displacement in the z-axis at the top end plate, as illustrated in Figure 2.

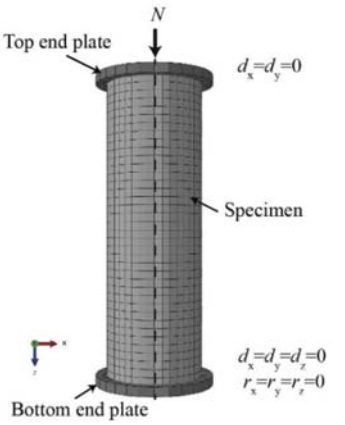

Figure 2. Load applications and boundary conditions.

2.2 *Verification of finite element models*

The FEMs of CDG and SDG CFST stub columns information were listed in Table 1.

3 INFLUENCE OF DIFFERENT DEBONDING GAP TYPES WITH SAME RD

3.1 *Parameters selection*

According to GB 50923-2013 (MOHURD 2013), when the R_{CDG} is larger than 0.2 or the T_{CDG} is larger than 3 mm, it is recommended to drill holes on the steel tube in DG range and grout. Therefore, in this research the maximum R_D was set at 0.2 and T_{CDG} was set as 3 mm. T_{SDG} was changed from 0 to 21 mm with an increment of 1 mm, and the corresponding χ_{SDG} changed from 0 to 9.1%. The corresponding R_{SDG} could be calculated according to the known T_{SDG}. The D of 219 mm, t of 4 mm, L of 657 mm were chosen. The cross-sections of SDG and CDG CFST columns with R_{SDG} = R_{CDG} were shown in Figure 3. For the material properties of steel, a yield strength (f_y) of 345 MPa. For the material properties of concrete, a characteristic strength (f_{ck}) of 32.4 MPa, cylinder strength (f_c') of 41.5 MPa.

3.2 *Ultimate load-bearing capacity*

In order to understand the influence of debonding gap on N_u, a reduction coefficient of N_u (K_D= $N_{u\text{-}D}/N_{u\text{-}N}$) was defined (Xue et al. 2012). The $N_{u\text{-}D}$ was the N_u of specimens with debonding gap (CDG or SDG specimen) and $N_{u\text{-}N}$ was the N_u of specimen without debonding gap (NDG specimen).

Table 1. Experimental and numerical results of CFST stub columns with CDG or SDG.

Debonding gap type	Literature	Label	N_u (kN)		
			$N_{u\text{-EXP}}$	$N_{u\text{-FEM}}$	$N_{u\text{-FEM}}/N_{u\text{-EXP}}$
CDG	Xue et al. (2012)	N3-0-A	2647	2705	1.02
		D3-1-A	2433	2431	0.99
		D3-2-A	2306	2358	1.02
		D3-3-A	2281	2345	1.02
		N4-0-A	2896	2965	1.02
		D4-1-A	2602	2625	1.00
		D4-2-A	2538	2554	1.00
		D4-3-A	2503	2532	1.01
	Han et al. (2016)	N-1	1559	1428	0.92
		N-2	1544		0.92
		C1.1-1	1143	1164	1.02
		C1.1-2	1113		1.05
		C2.2-1	1068	1143	1.07
		C2.2-2	1041		1.10
SDG	Liang (2008)	PX-0-0	3400	3385	0.99
		PX-0-2	3130	3010	1.04
		PX-0-5	3010	3022	1.00
	Guo et al. (2020)	A0C0	5582	5809	1.04
		A0C6.42	5476	5236	0.96
	Zhang et al. (2019)	C0-0-0a	1779	1708	0.96
		C0-0-0b	1722		0.99
		CS-6-0a	1569	1467	0.93
		CS-6-0b	1518		0.97

The N_u obtained by experimental tests ($N_{u\text{-EXP}}$) and FEMs ($N_{u\text{-FEM}}$) were compared, as listed in Table 1. The mean value of $N_{u\text{-FEM}}/N_{u\text{-EXP}}$ was 1.001 and the standard deviation was 0.045. Therefore, the finite element simulation method could be used to simulate the mechanical performance of CDG and SDG CFST stub columns.

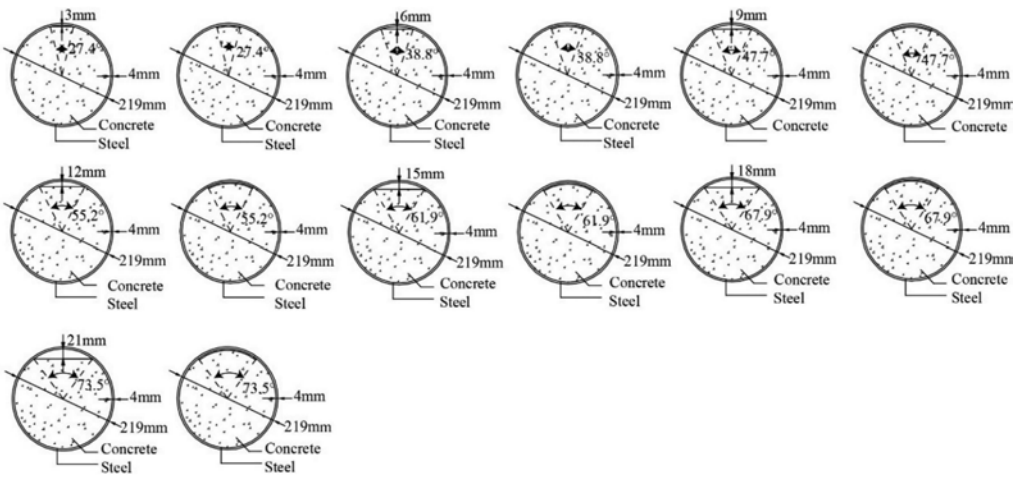

Figure 3. Cross-sections of SDG and CDG specimens with same R_D.

The influence of different debonding types with the same R_D on the N_u, K_D and the decrease rate of K_D are shown in Figure 4. It can be found that with an increase in R_D, the N_u and K_D of CDG or SDG specimens decreased. A critical R_D ($R_{D\text{-cr}}$) (0.12) can be found. When $R_D \leq R_{D\text{-cr}}$, with an increase in R_D, the influence of different debonding types no N_u and K_D was negligible, and the minimum K_D was 0.94. When $R_D > R_{D\text{-cr}}$, with an increase in

R_D, the influence of different debonding types on N_u and K_D was different; the N_u and K_D of SDG specimens decreased linearly, however, the N_u and K_D of CDG specimens decreased nonlinearly with gradually reduced decrease rates, as shown in Figure 4a. When $R_D = 0.2$, for CDG specimen, the N_u decreased from 3005 kN to 2674 kN and the K_D decreased to 0.89; for SDG specimen, the N_u decreased from 3005 kN to 2597 kN and the K_D decreased to 0.86. With an increase in R_D, the decrease rate of K_D for CDG or SDG specimens increased firstly until the R_D reached 0.09 and the maximum decrease rate of K_D was 0.014; when $R_D > 0.09$, the decrease rate of K_D for CDG or SDG specimens decreased, as showed in Figure 4b, the decrease ratio of K_D of CDG specimen reduced faster than that of SDG specimen.

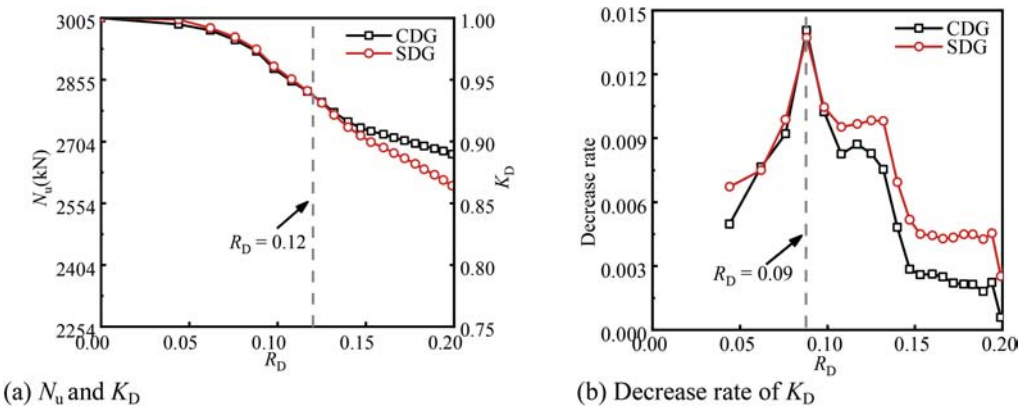

Figure 4. Influence of different debonding gap types on N_u, K_D, and decrease rate of K_D.

3.3 *Axial load-axial displacement curves*

The comparisons of the axial load (N)-axial displacement (Δ) relationship curves of different NDG or DG specimens (CDG and SDG specimens) are shown in Figure 5. It can be found that when $R_D = 0.12$, the influence of different debonding gap types on the $N_{u\text{-}D}$ and the curves was negligible. When $R_D = 0.2$, the difference of N-Δ relationship curves of CDG or SDG specimens was the descending stage after $N_{u\text{-}D}$. For CDG specimen, the N decreased until nearly $A_s f_y + A_c f_c'$; for SDG specimen, the descending branch of the N-Δ relationship curves was longer than that of CDG specimen, and the N decreased to a value less than $A_s f_y + A_c f_c'$. It is because even the R_D was the same (0.2), the T_{CDG} (3 mm) was less than the T_{SDG} (20 mm). Therefore, the inward buckling in CDG specimen can easier let the steel tube and concrete core in DG range contact and provide contact stress to partial concrete core in DG range from the steel tube than that of SDG specimen.

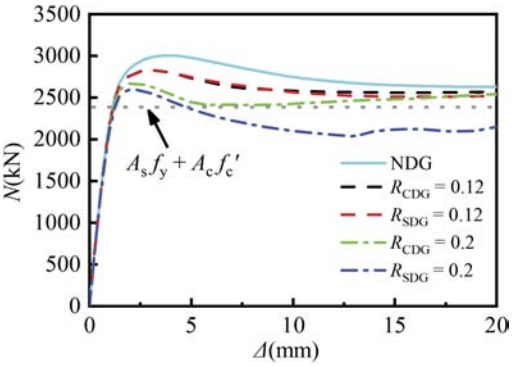

Figure 5. Comparisons of N-Δ relationship curves of NDG or different DG specimens.

3.4 *Failure mode*

The CDG or SDG range and NDG range in the cross-section of the specimen were defined in Figure 6.

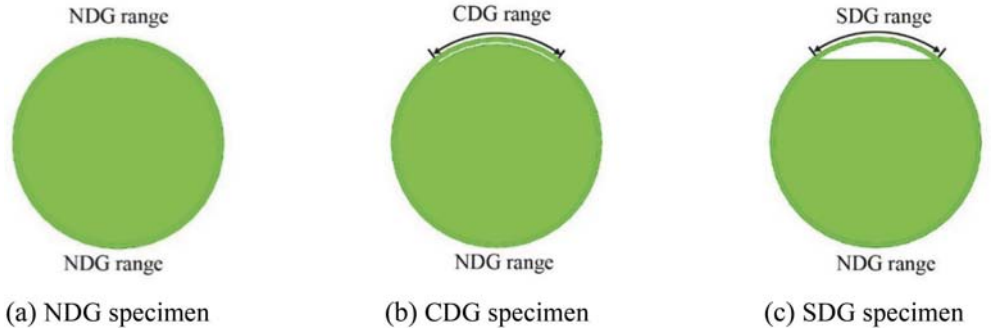

Figure 6. Debonding or non-debonding ranges in cross-section.

The failure modes of axially compressed CDG or SDG CFST stub columns with the same R_D were showed in Figure 7. When $R_D = 0.12$, the inward buckling in DG range (CDG and SDG range), overall bending in NDG range, and lightly elephant-foot shape buckling at both ends were observed in CDG or SDG specimens, as shown in Figures 7a, b. When $R_D = 0.2$, the overall bending in NDG range and elephant-foot shape buckling at both ends can be observed in CDG or SDG specimens; however, in DG range, the inward buckling was observed in CDG specimen, while wavy inward and outward local buckling was observed in SDG specimen, as shown in Figures 7c, d.

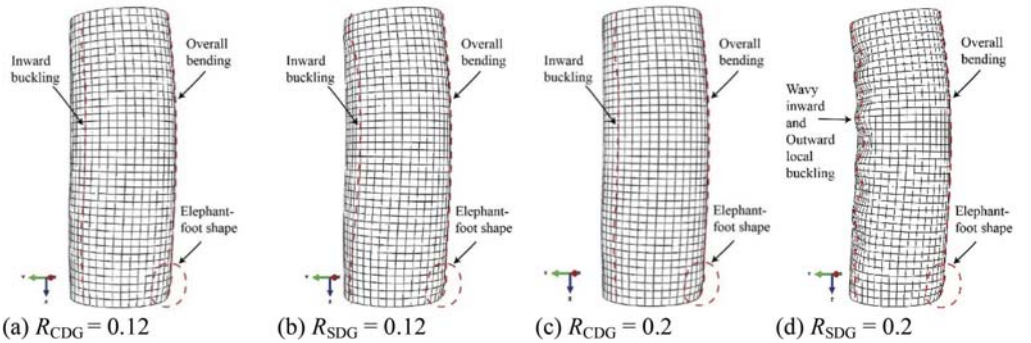

Figure 7. Failure modes of SDG and CDG specimens with same R_D.

The lateral deflection (U) curves along the L of different specimens corresponding to N_u were illustrated in Figures 8a, c. The $R_D = 0.12$, $R_D = 0.2$ and NDG specimens were compared. The U away from the center of the specimen was defined as the positive and the U towards the center of the specimen was defined as the negative. The NDG and DG range in the specimen were illustrated in Figure 8b, where the NDG range is in the right and the DG range (DG specimen) or NDG range (NDG specimen) is in the left.

By comparing the U of DG specimens and NDG specimen, the overall bending toward to DG range can be found in DG specimen, and the outward buckling can be found in NDG specimen.

By comparing the U at the $L/2$ in DG range ($U_{L/2\text{-}D}$) of different specimens (Figure 8a), it could be found that when the R_{CDG} increased from 0.12 to 0.2, the $U_{L/2\text{-}D}$ decreased from 0.66 to 0.51 mm (by 0.15 mm). When the R_{SDG} increased from 0.12 to 0.2, the $U_{L/2\text{-}D}$ slightly increased from 0.65 to 0.70 mm (by 0.05 mm). When $R_D = 0.12$, the $U_{L/2\text{-}D}$ of CDG or SDG specimens

were nearly the same, therefore, the influence of different debonding gap types on the $U_{L/2\text{-}D}$ is small. When R_D = 0.2, the $U_{L/2\text{-}D}$ of CDG specimen was smaller than that of SDG specimen, it is because that the inward buckling in SDG specimen was more serious than that in CDG specimen.

By comparing the U at the $L/2$ in NDG range ($U_{L/2\text{-}N}$) of different specimens (Figure 8c), it could be found that with an increase in R_D, the $U_{L/2\text{-}N}$ decreased. When the R_{CDG} increased from 0.12 to 0.2, the $U_{L/2\text{-}N}$ decreased from 0.65 to 0.35 mm (by 0.3 mm). When the R_{SDG} increased from 0.12 to 0.2, the $U_{L/2\text{-}N}$ slightly decreased from 0.64 to 0.53 mm (by 0.11 mm). When R_D = 0.12, the $U_{L/2\text{-}N}$ of CDG or SDG specimens were nearly the same, therefore, the influence of different debonding gap types on the $U_{L/2\text{-}N}$ was small. When R_D = 0.2, the $U_{L/2\text{-}N}$ of CDG specimen was smaller than that of SDG specimens, therefore, the overall bending in SDG specimen was more serious than that in CDG specimen.

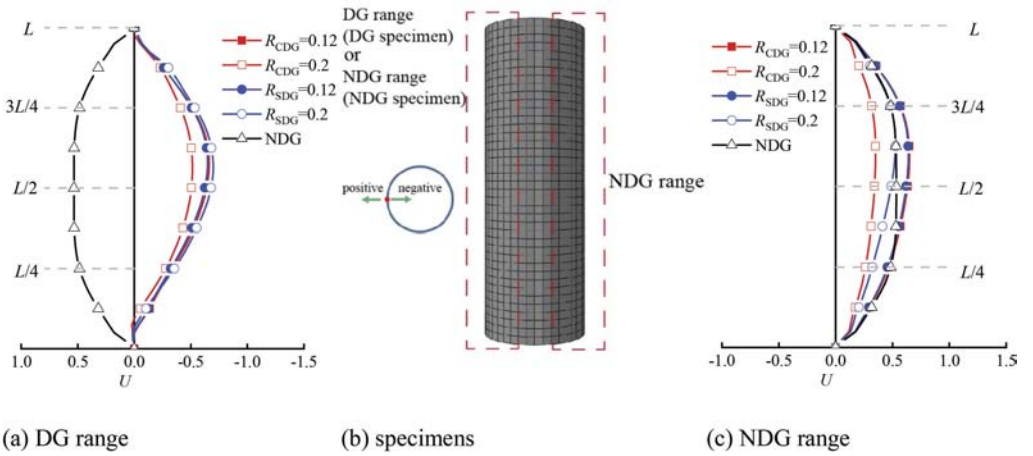

Figure 8. Lateral deflections corresponding to N_u.

4 CONCLUSIONS

Based on the finite element analyses, the following conclusions can be drawn:

(1) With an increase in debonding parameters, the ultimate load-bearing capacity of axially compressed CFST stub columns decreased. The critical value of debonding arc-length ratio could be obtained. When the debonding arc-length ratio was less than the critical value (0.12), the influence of different debonding types on load bearing capacity was negligible. When the debonding arc-length ratio was greater than the critical value (0.12), the load bearing capacity of SDG specimen decreased linearly, however, CDG specimen decreased nonlinearly with gradually reduced decrease rates.

(2) When the debonding arc-length ratio was 0.12, the influence of different debonding gap types on the load-displacement curve was negligible. When the debonding arc-length was 0.2, the descending stage after N_u in SDG specimen was longer than CDG specimen.

(3) When the debonding arc-length ratio was less than the critical value (0.12), the influence of different debonding gap types on the failure mode was negligible. The failure modes of steel tubes shows that the inward buckling in debonding range, and overall bending in non-debonding range. When the debonding arc-length ratio reached 0.2, the failure mode had no obvious change in CDG specimen, but the wavy inward and outward local buckling could be observed in SDG specimen.

(4) When the debonding arc-length ratio was less than the critical value (0.12), the influence of different debonding gap types on the lateral deflections was negligible. However, when debonding arc-length ratio was 0.2, both inward buckling in DG range and overall bending in NDG range of SDG was more serious than CDG, wavy inward and outward local buckling could be observed in DG range of SDG specimen.

(5) The constraint effect between steel tube and concrete was the key to influence the ultimate bearing capacity of CFST axially compresses stub columns. The next step of the research is to analyze the influence of different debonding types on the constraint effect between steel tube and concrete.

ACKNOWLEDGEMENTS

This research was supported by the National Natural Science Foundation of China (grant numbers 51508103 and 51778148), the Open Project of Fujian Provincial Key Laboratory on Multi-Disasters Prevention and Mitigation in Civil Engineering (MPMC-2022-4) and the Open Project Fund of the Sustainable and Innovative Bridge Engineering Research Center of Fujian Province University, Grant No. SIBERC 202203.

REFERENCES

Chen, S.M. & Zhang, H.F. 2012. Numerical analysis of the axially loaded concrete filled steel tube columns with debonding separation at the steel-concrete interface. *Steel Composite Structures* 13(3): 277–293.

Contento, A., Aloisio, A., Xue, J.Q., Quaranta, G., Briseghella, B. & Gardoni, P. 2022.Probabilistic axial capacity model for concrete-filled steel tubes accounting for load eccentricity and debonding. *Engineering Structures* 268: 114730.

Guo, C. & Lu, Z. 2020. Air void and cap gap composite defects of concrete-filled steel-tube arch bridge transverse brace. *Journal of Performance of Constructed Facilities* 34(4): 04020073.

Han, L.H., Ye, Y. & Liao, F.Y. 2016. Effects of core concrete initial imperfection on performance of eccentrically loaded CFST columns. *Journal of Structural Engineering* 142(12): 04016132.

Liang, K.F. 2008. *Effect of debonding on mechanical properties of concrete-filled steel tube*. Changsha: Hu'nan University.

Liao, F.Y., Han, L.H. & He, S.H. 2011. Behavior of CFST short column and beam with initial concrete imperfection: Experiments. *Journal of Constructional Steel Research* 67(12): 1922–1935.

Liao, F.Y., Han, L.H. & He, S.H. 2011. Behavior of CFST stub column with initial concrete imperfection: Analysis and calculations. *Thin-Walled Structures* 70:57–69.

Ministry of Housing and Urban-Rural Development of the People's Republic of China (MOHURD). 2013. *Technical specification for concrete-filled steel tube arch bridges*. Beijing: China Planning Press.

Schnabl, S. & Planinc, I. 2018. Circumferential gap and partial debonding effects on buckling loads and modes of slender CFST circular columns. *Acta Mechanica* 230: 909–928.

Shao, Z.X., Ren, G.F. & Fang, Y.X. 2018. Reinforce technical analysis of concrete-filled steel tube with cementation deviating. *Journal of Guangxi University (Natural Science Edition)* 43(1): 126–131.

Xie X. 2020. *Effect of Core Concrete Defects on Mechanical Properties of Ordinary Circular Steel Tube Concrete Axial Compression Components*. Sichuan, China: Southwest University of Science and Technology.

Xue, J.Q., Briseghella, B. & Chen, B.C. 2012. Effects of debonding on circular CFST stub columns. *Journal of Constructional Steel Research* 69(1): 64–76.

Xue, J.Q., Chen, B.C. & Briseghella, B. 2010. Experimental research on debonding in concrete-filled steel tubes columns subjected to eccentric loading. *IABSE Symposium Report 2010*: 40–47. Switzerland: IABSE.

Xue, J.Q., Fiore, A., Liu, Z.H., Briseghella, B. & Marano, G.C. 2021a. Prediction of ultimate load capacities of CFST columns with debonding by EPR. *Thin-Walled Structures* 164: 107912.

Xue, J.Q., Huang, J.P., Briseghella. B. & Huang, F.Y. 2022. Influence of different debonding gap types on mechanical performance of axially loaded CFST stub columns. *IABSE Congress Nanjing 2022 Report*: 1600–1608. Switzerland: IABSE.

Xue, J.Q., Liu, Z.H., Zhang, Y.F., Briseghella, B., Chen, B.C. & Wei, J.G. 2021b. Experimental research on influence of debonding on circular CFST long columns subjected to eccentric load. *IALCCE2020*: 1481–1485. Florida: CRC Press.

Xue, J.Q., Zhang, Y.F., Briseghella, B. & Chen, B.C. 2020. Experimental Research on Effects of Debonding on Circular CFST Columns with Different Slenderness Ratios. *Proceedings of ARCH 2019*: 369–377. Switzerland: Springer.

Zhang, K.K., Liao, F.Y. & Huang, Z.W. 2019. Study on axial compression behavior of CFRP reinforced short concrete-filled steel tube (CFST) columns with spherical-cap debonding. *Journal of Building Structures* 40(S1): 227–232.